Mon. Not. R. astr. Soc. (1989) **239,** 153–171

Rapidly rotating general relativistic stars – II. Differentially rotating polytropes

Hidemi Komatsu,★[1] Yoshiharu Eriguchi[2] & Izumi Hachisu[3]

[1] *Department of Astronomy, Faculty of Science, University of Tokyo, Yayoi, Bunkyo-ku, Tokyo 113, Japan*

[2] *Department of Earth Science and Astronomy, College of Arts and Sciences, University of Tokyo, Komaba, Meguro-ku, Tokyo 153, Japan*

[3] *Department of Aeronautical Engineering, Kyoto University, Yoshida-honmachi, Sakyo-ku, Kyoto 606, Japan*

Accepted 1989 January 17. Received 1988 December 2; in original form 1988 August 8

Summary. We have applied the numerical method which was developed for Newtonian gravity to general relativistic, differentially rotating bodies including ring-like structures. A number of equilibrium structures are obtained for two different polytropic indices $N=1/2$ and $N=3/2$, because the various proposed equations of state for the nuclear density region fall into the range $N=1/2$ to $3/2$ from the viewpoint of its softness.

Each modelled sequence is specified by three parameters: the polytropic index N, the strength of gravity $\kappa=p_{\max}/\varepsilon_{\max}c^2$ and the rotation parameter A. Here $p_{\max}$ is the maximum pressure, $\varepsilon_{\max}$ the maximum energy density. For a large value of A, the rotation law approaches that for a rigid rotation. For a small value of A, the rotation law becomes that for j-constant rotation, where j is the specific angular momentum measured by the proper time of matter. We have computed 10 sequences for $N=3/2$ polytropes and 9 sequences for $N=1/2$ polytropes with various values of κ and A. For both the strong (general relativistic) and weak (Newtonian) gravities, models including two limiting cases of nearly rigid rotation and strongly differential rotation are obtained.

We have found (i) that the non-dimensional quantity

$$F=(J^{6-2N}/K^N)^{1/(10-4N)}/M$$

is a good parameter to classify the equilibrium structures, where J is the total angular momentum, M the gravitational mass and K the polytropic constant, (ii) that the ratio of the rotational to the gravitational energy $T/|W|$ increases as κ

★ Presented as a part of the first author's thesis for the PhD degree of the Department of Astronomy, University of Tokyo.

becomes large for the same value of F, and (iii) that the increase in the gravitational mass by rotation is considerably suppressed in the strong-gravity limit.

1 Introduction

It has been widely accepted that neutron stars are born in supernova explosions or through accretion-induced collapse of heavy white dwarfs. If an iron core just before collapse is rapidly rotating, then the collapsed high-density matter has a very flat structure and its rotation law is strongly differential (Symbalisty 1984). Such objects reach a quasi-static structure and cool down due to neutrino loss. If this transient structure becomes dynamically unstable to non-axisymmetric modes in the process of cooling, a proto-neutron star may fragment and finally merge again into one body radiating gravitational waves. Such an instability may produce the second neutrino pulse, as observed with the Kamiokande II detector (Hirata *et al.* 1987; Nakamura & Fukugita 1987). Relativistic and differentially rotating hydrostatic structures are expected to appear in such a situation.

Differentially rotating and fully general relativistic configurations were examined first by Wilson (1972, 1973); he also demonstrated that ergo regions do exist. However, his work is intermediately successful because he assumed too restrictive density distributions. His formulation has another drawback in that his code cannot guarantee that proper solutions for highly deformed and highly relativistic configurations such as tori will be obtained, because his boundary condition does not satisfy the asymptotic condition exactly.

We have already developed a powerful numerical method in a previous paper which is improved to exactly satisfy the boundary condition at the asymptotic region (Komatsu, Eriguchi & Hachisu 1989, hereafter Paper I). In that paper, we have detailed our numerical method and mentioned the results of the rigid-rotation case. However, for uniformly rotating configurations, deformation from the sphere is so small that crucial effects of rotation cannot be fully studied. In the present paper, therefore, we describe differentially rotating models. In Section 2, numerical models are presented for two cases of the polytropic index, i.e. $N=1/2$ and $N=3/2$. Our result shows that the increase in the gravitational mass is considerably suppressed, even if toroidal configurations are investigated. This fact is very contrasting with the Newtonian limit. For Newtonian gravity there exist ring equilibrium configurations whose outer radius from the rotation axis is very large compared with the size of the cross-section of the ring (Eriguchi & Sugimoto 1981; Eriguchi & Hachisu 1985; Hachisu 1986). Such a ring with a large distance from the rotation axis can have a significantly large mass compared with a spherical model when the maximum density is fixed to be the same. However, for the general relativistic case, even if the angular momentum of the ring is rather large, it seems hard to be a large-distance ring. We will use the same notations as in Paper I throughout the present paper.

2 Equilibrium structures

We must specify four parameters to obtain an equilibrium model in our numerical method; these are the axis ratio r_p/r_e, polytropic index N, the ratio of the maximum pressure to the maximum energy density $\kappa = p_{max}/\varepsilon_{max}$, and the rotation parameter A. Here, r_p and r_e are the radii at the pole and at the equator, respectively (see fig. 1 of Paper I for details). Fixing three parameters of N, κ and A, we have obtained a set of solutions by changing the axis ratio r_p/r_e. We will, for simplicity, call this set of solutions the *equilibrium sequence.*

Although various equations of state have been proposed by many authors, their effective softness or hardness falls into the range of $N=1/2-3/2$ for the nuclear density region (see, e.g.

Friedman, Ipser & Parker 1986). Therefore, we have computed models only for the polytropic indices $N=1/2$ and $N=3/2$ as two limiting situations.

The parameter κ is an indicator of the strength of gravity. When the structure is centrally condensed, this parameter is a good representative of the strength of gravity. If the structure becomes ring-like, however, this is no longer a good parameter because even models with $M/r_e \sim 1$ have a relatively small value of $\kappa \sim 0.2$–0.3. Here, M and r_e are the gravitational mass and the equatorial outer radius of rings, respectively. Although we have computed only models with relatively small values of κ for differential rotation cases, some obtained models are in a highly relativistic state.

The other specifying parameter A denotes the degree of differential rotation. For a large value of A, the rotation law approaches that for a rigid rotation. For a small value of A, on the other hand, it approaches a j-constant rotation law, where j is the specific angular momentum measured by the proper time of matter (see Section 2.2 of Paper I for details).

We have computed 10 sequences for $N=3/2$ and nine sequences for $N=1/2$. Specifying parameters for each sequence are summarized in Table 1. For each value of κ, we have chosen the value of A so that the angular velocity distribution becomes similar from model to model in each subgroup of rotation in Table 1.

2.1 $N=3/2$ POLYTROPES

For the polytropic index $N=3/2$, we have computed 10 sequences having different values of κ and A, as seen in Table 1. Fig. 1(a) shows the energy density distribution ε for the model just at $r_p/r_e=0$ on sequence number 3 ($\kappa=0.1$ and $A=0.6$). In order to compare it with a structure of Newtonian limit, we plot a structure of a model on sequence number 1 ($\kappa=0.001$ and $A=0.065$) in Fig. 1(b). It is clear that the strong gravity gathers matter inward. In Fig. 1(a), we plot the gravitational radius $r_g=M/2$. The bulk of the ring resides outside the gravitational radius.

Table 1. Specifying parameters of modelled sequences.

sequence	N	κ	A	*comments*
1	3/2	0.001	0.065	
2	3/2	0.05	0.45	nearly rigid rotation
3	3/2	0.1	0.6	
4	3/2	0.001	0.031	intermediately
5	3/2	0.1	0.29	differential rotation
6	3/2	0.2	0.39	
7	3/2	0.001	0.0125	
8	3/2	0.1	0.155	strongly differential
9	3/2	0.2	0.25	rotation
10	3/2	0.4	0.4	
11	1/2	0.001	0.036	
12	1/2	0.1	0.35	nearly rigid rotation
13	1/2	1/3	0.55	
14	1/2	0.001	0.018	intermediately
15	1/2	0.1	0.17	differential rotation
16	1/2	1/3	0.27	
17	1/2	0.001	0.0064	strongly differential
18	1/2	0.1	0.076	rotation
19	1/2	1/3	0.16	

Fig. 1(c) and (d) correspond to the energy density distributions for the strongly differential rotation case, i.e. models at $r_p/r_e = 0$ on sequences number 10 ($\kappa = 0.4$ and $A = 0.4$) and number 7 ($\kappa = 0.001$ and $A = 0.0125$), respectively. In this case, it is much clearer than in the nearly rigid rotation case that the strong gravity gathers matter towards the rotation axis. As a result, the bulk of the torus is inside the gravitational radius, as seen in Fig. 1(c).

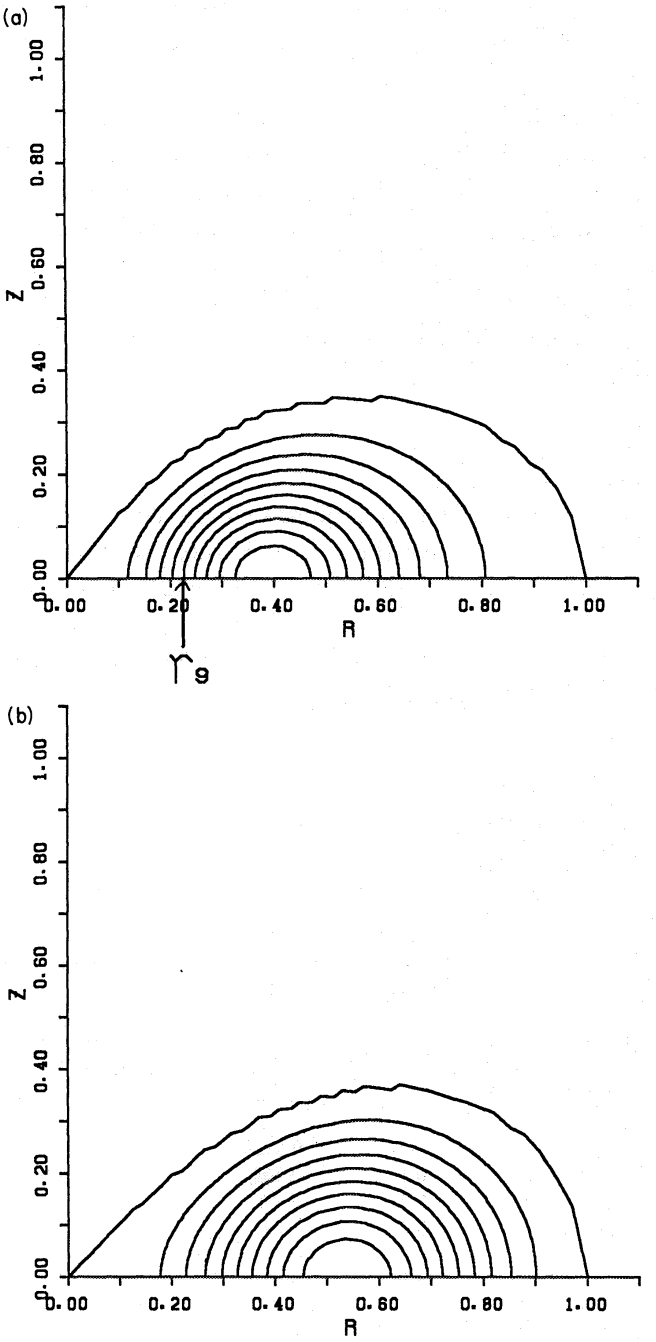

Figure 1. Meridional cross-sections of the energy density are shown for four ring-like models at $r_p/r_e = 0$ in the case of $N = 3/2$: (a) strong gravity and nearly rigid rotation model (on sequence number 3; $\kappa = 0.1$ and $A = 0.6$); (b) Newtonian limit and nearly rigid rotation model (on sequence number 1; $\kappa = 0.001$ and $A = 0.065$); (c) strong gravity and strongly differential rotation model (on sequence number 10; $\kappa = 0.4$ and $A = 0.4$); (d) Newtonian limit and strongly differential rotation model (on sequence number 7; $\kappa = 0.001$ and $A = 0.0125$). Contours are linearly spaced by 0.1 ε_{max}. The gravitational radius $r_g = M/2$ is also plotted for two strong-gravity cases (a) and (c). It is clear that the strong gravity gathers matter towards the rotation axis.

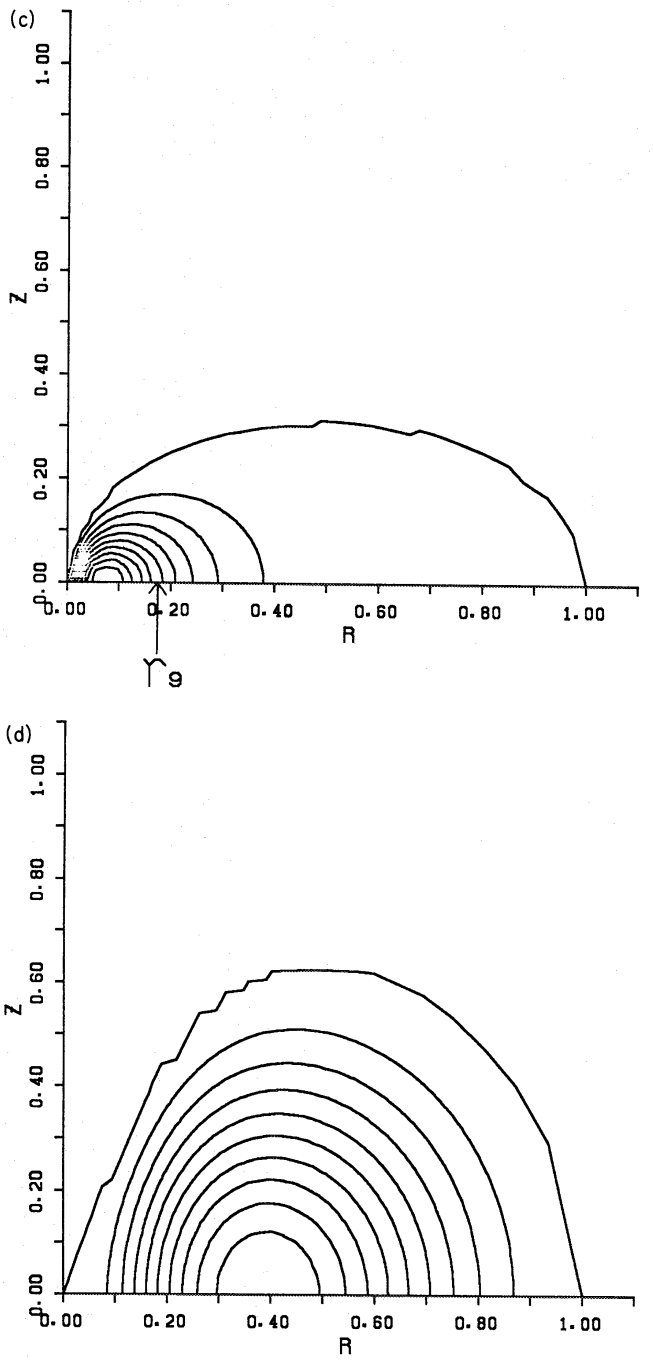

Figure 1 – *continued*

We have plotted our 10 sequences in the F–$T/|W|$ plane (Fig. 2), where F is a globally almost conserved, non-dimensional quantity during the adiabatic and axisymmetric collapse (Tohline 1984; Eriguchi & Müller 1985) which is defined by

$$F = J^{(3-N)/(5-2N)}/(K^{N/(10-4N)}M), \tag{1}$$

and T and W are the rotational and gravitational energy, respectively (see Paper I for their exact definitions). It should be noted that this definition of F is slightly different from those used by Tohline or Eriguchi & Müller. If we assume that the equation of state is fixed during the collapse (this means that the polytropic constant K and the polytropic index N are constant

both in time and in space), the non-dimensional value of F is almost constant during the axisymmetric collapse apart from the mass decrease corresponding to the energy radiated away by the gravitational radiation, which has been estimated to be very small for axially symmetric collapse (Stark & Piran 1985). Therefore, if we specify the initial value of F and the local angular momentum distribution, we can easily find the final state of the collapsing matter

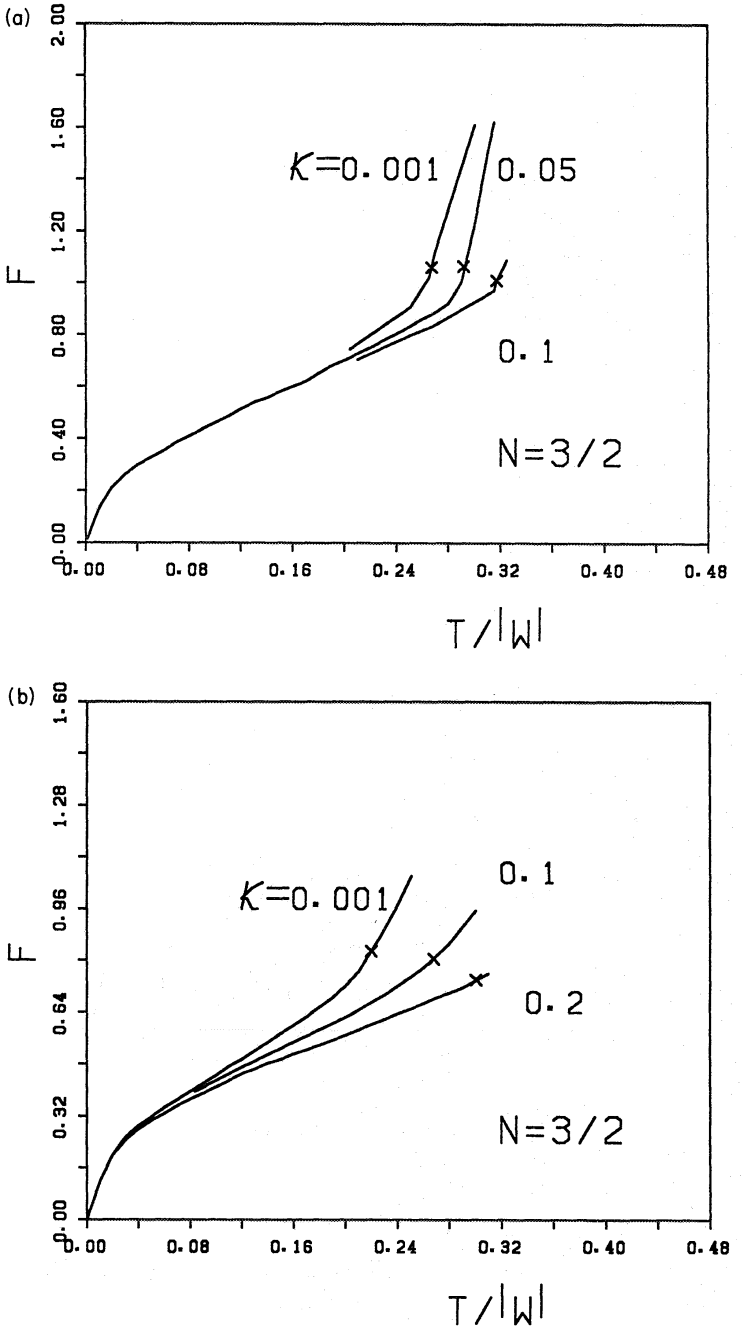

Figure 2. The F value is plotted against the ratio of the rotational to the gravitational energy $T/|W|$ for various equilibrium sequences in the case of $N=3/2$: (a) nearly rigid rotation case; (b) intermediately differential rotation case; (c) strongly differential rotation case. Crosses denote the models at $r_p/r_c=0$. The curvature of each locus drastically changes at the transition point from a centrally condensed structure to a ring-like one near the cross in (a). In (b) the structure smoothly changes to a ring-like one. In (c) all the structures are essentially ring-like throughout the sequence, except the region where $T/|W|\sim 0$.

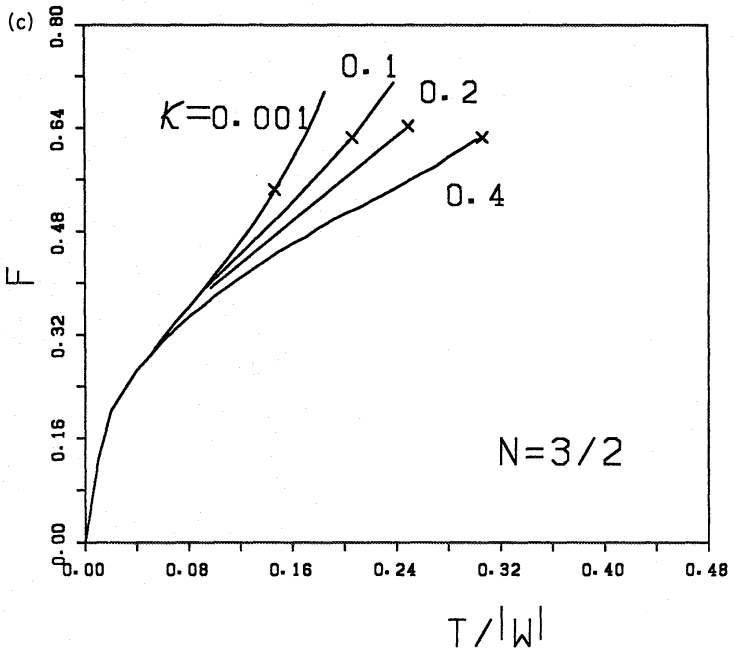

Figure 2 – *continued*

(see, e.g. Hachisu, Tohline & Eriguchi 1987, 1988 for the Newtonian limit). In this sense, the F value is a physical meaningful quantity to predict the final state of collapse from the initial state. On the other hand, the $T/|W|$ value is used as a simple stability indicator for the Newtonian limit. For centrally condensed, rotating objects, dynamical instability against a non-axisymmetric $m=2$ mode occurs around $T/|W|=0.27$ in the Newtonian limit. For ring-like objects, the same type of dynamical instability occurs around $T/|W|=0.14$–0.16. (See Hachisu *et al.* 1987, 1988 for details.)

For the same F value, the strong-gravity models have a larger $T/|W|$ value than that for the weak gravity. We have not plotted the sequences having $\kappa \geq 0.2$ for near-rigid rotation, because the sequences are terminated by mass-shedding from the equatorial surface. Here the term 'mass-shedding' means that the centrifugal force surmounts the gravity at the equatorial surface and, as a result, matter is shed from the equatorial surface. From Fig. 2(a), we can observe that the configuration change from a centrally condensed type to a ring-like one occurs at almost the same value of $F \sim 1.0$. (Crosses correspond to the models having $r_p/r_e = 0$.) Since we expect that the ring-like structure is dynamically unstable against non-axisymmetric modes because their $T/|W|$-values are much larger than 0.16, we can further speculate that these ring-like structures can fragment into pieces. Therefore, if we use the F value instead of the $T/|W|$-value, the fragmentation criterion may be given by a unique value of F, regardless of the strength of gravity. Roughly speaking, if the F value of the initial stage is larger than ~ 1 and $J/M^2 > 1$, we can expect that the collapsing matter will experience a fragmentation or, at least, a non-axisymmetric deformation. If we choose initially $J/M^2 \leq 1$, there is another possibility that the collapsing system will result in a black hole before the system can fragment (Nakamura 1981). Of course, we must examine the dynamical stability of the obtained models in order to answer finally under what initial conditions the collapsing matter can fragment or can deform non-axisymmetrically.

In Fig. 3 are plotted the increase in the gravitational mass $(M-M_s)/M_s$ against $T/|W|$, where M_s is the gravitational mass of the non-rotating spherical model having the same κ. Fig. 3(a) corresponds to the nearly rigid rotation case and Fig. 3(b) corresponds to the strongly

differential rotation case. It is clear that the mass increase in the strong-gravity cases is much smaller than that in the weak-gravity ones with the same $T/|W|$ value. This is because the strong gravity concentrates matter into a small region and rotation must be stronger to support the matter against such a strong gravity. This effect increases the rotational energy much more than in the weak gravity case.

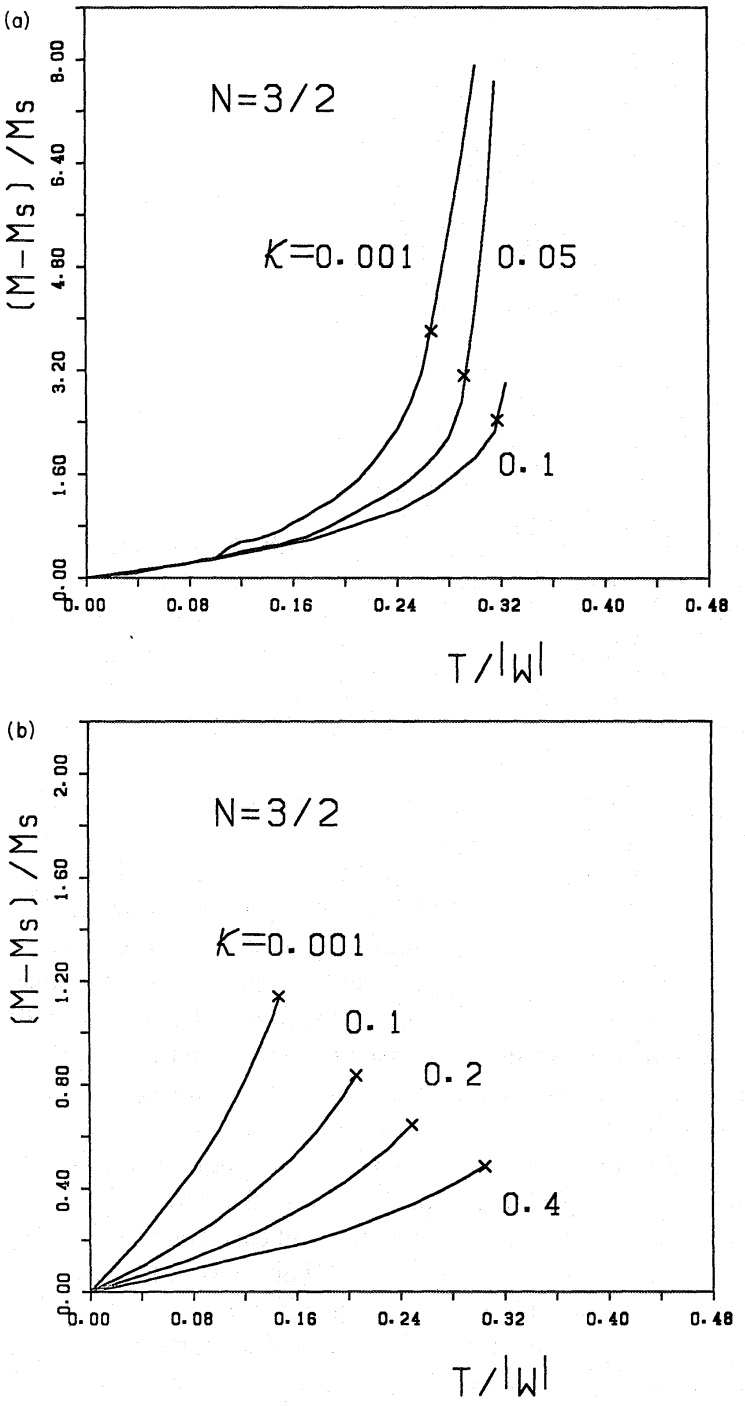

Figure 3. The increase in the gravitational mass $(M-M_s)/M_s$ is plotted against $T/|W|$ for the $N=3/2$ polytropes, where M_s is the gravitational mass of the spherically symmetric model having the same value of κ. (a) Nearly rigid rotation case; (b) strongly differential rotation case. The specifying parameter is attached to each curve. Crosses denote the models at $r_p/r_e=0$.

2.2 $N=1/2$ POLYTROPES

We have computed nine sequences having different values of κ and A, as tabulated in Table 1. Fig. 4 shows the energy-density distributions in the meridional plane when $r_p/r_e=0$ is reached. Fig. 4(a) corresponds to the model of nearly rigid rotation and strong gravity ($\kappa=1/3$ and $A=0.55$; sequence number 13). The sound velocity derived from the equation of state is

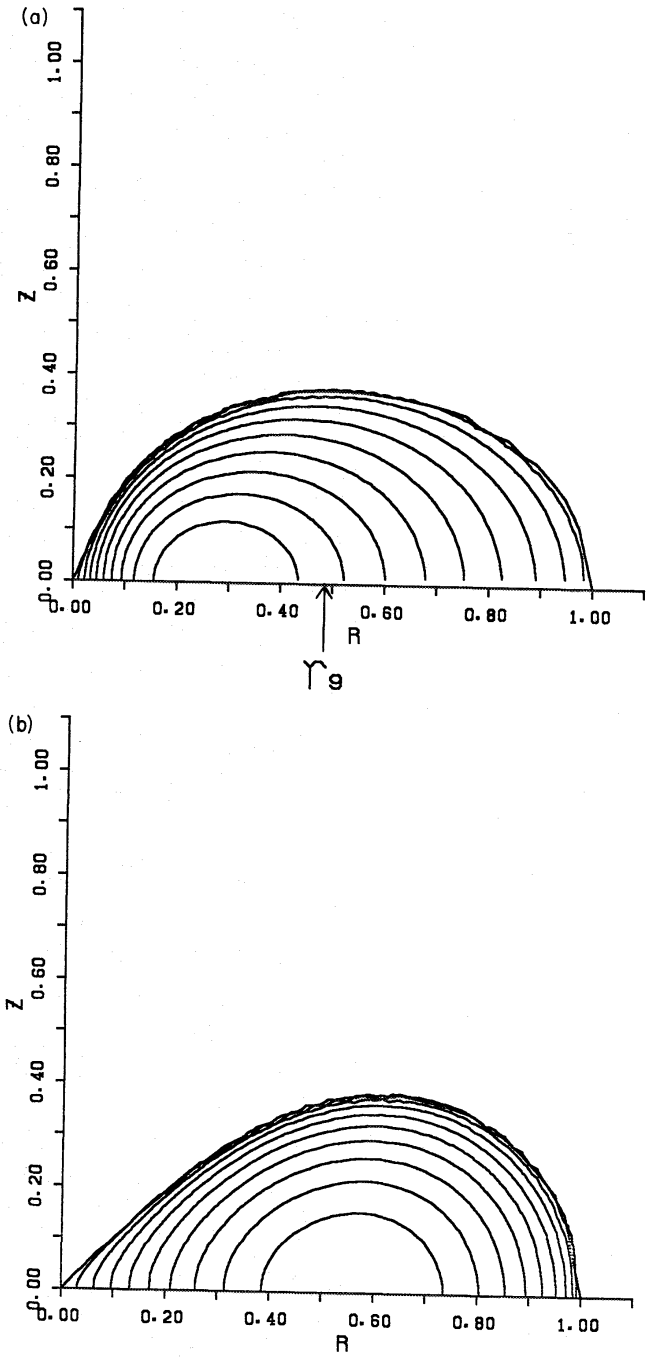

Figure 4. Same as Fig. 1, but for $N=1/2$ sequences: (a) strong gravity and nearly rigid rotation case (on sequence number 13; $\kappa=1/3$ and $A=0.55$); (b) Newtonian limit and nearly rigid rotation case (on sequence number 11; $\kappa=0.001$ and $A=0.036$); (c) strong gravity and strongly differential rotation case (on sequence number 19; $\kappa=1/3$ and $A=0.16$); (d) Newtonian limit and strongly differential rotation case (on sequence number 17; $\kappa=0.001$ and $A=0.0064$).

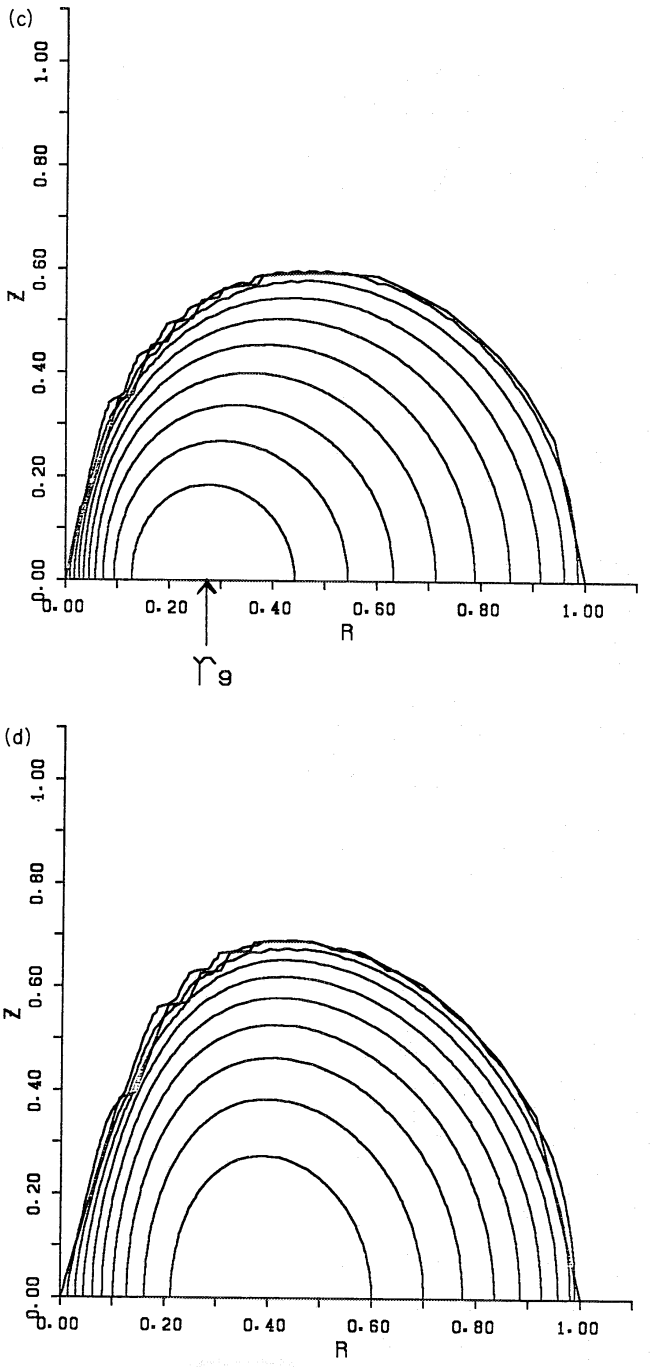

Figure 4 – *continued*

$c_s=(dp/d\varepsilon)^{1/2}$ and, hence, the maximum sound velocity is attained at the maximum energy density point, i.e. $c_{s,\max}=[(1+1/N)\kappa]^{1/2}$. When $N=1/2$ and $\kappa=1/3$, the maximum sound velocity reaches the light velocity. For comparison, we also plot the energy density distribution of the Newtonian limit (Fig. 4b). The fact that the strong gravity gathers matter towards the centre is also clearly observed. In Fig. 4(c) and (d) the cross sections of tori are shown for the case of strongly differential rotation. The shapes of tori are very fat compared with the case of nearly rigid rotation and the same tendency of the strong gravity to gather matter is also observed.

The dimensionless quantity F is plotted against $T/|W|$ for three types of rotation laws in Fig. 5: (a) nearly rigid rotation; (b) intermediately differential rotation; (c) strongly differential rotation. Crosses denote the models just at $r_p/r_e = 0$. The F–$T/|W|$ relations are almost the same, regardless of the rotation law. Independently of the strength of gravity, the configuration changes from spheroidal to toroidal at $F \sim 0.7$ from Fig. 5(a).

Fig. 6 shows the increase in the gravitational mass for the case of nearly rigid rotation. Of course, this increase in the gravitational mass by rotation depends on the rotation law but its dependency is much smaller than the κ-dependency. Therefore, we plot only the rigid-rotation

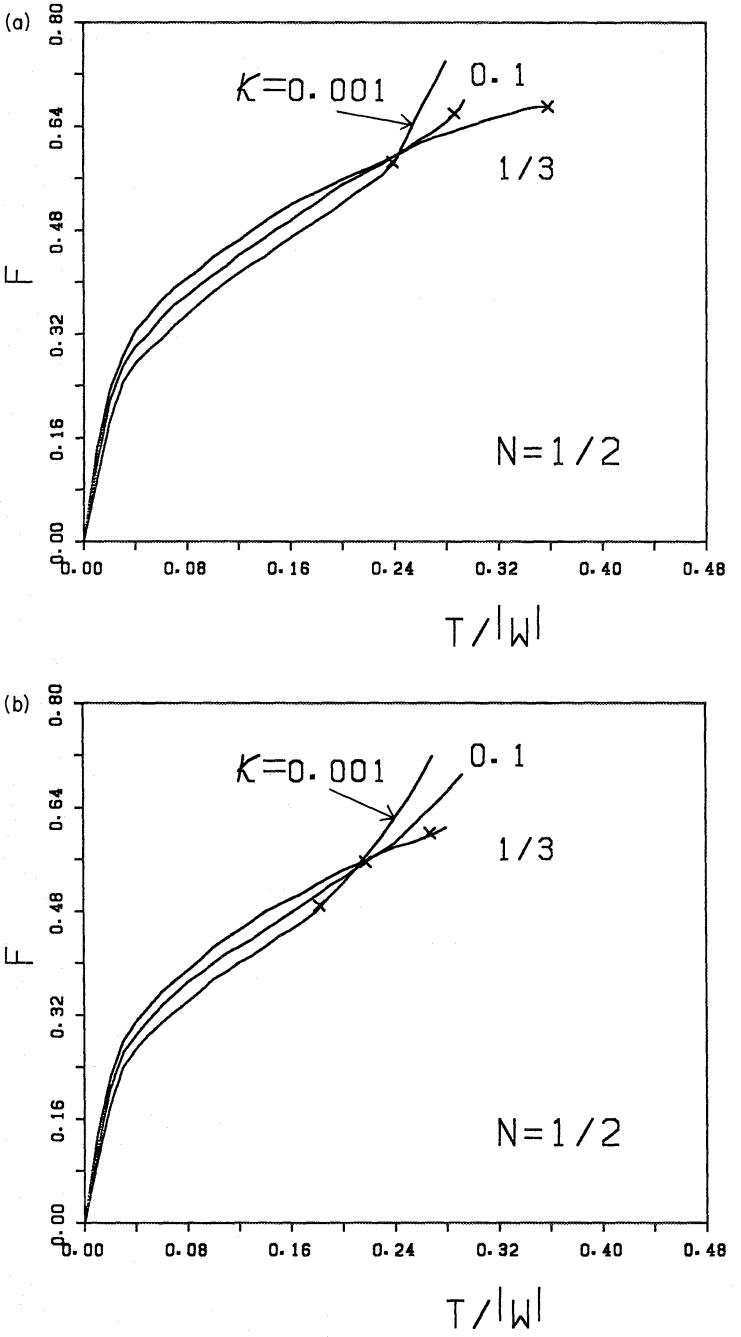

Figure 5. Same as Fig. 2, but for $N = 1/2$ sequences: (a) nearly rigid rotation case; (b) intermediately differential rotation case; (c) strongly differential rotation case.

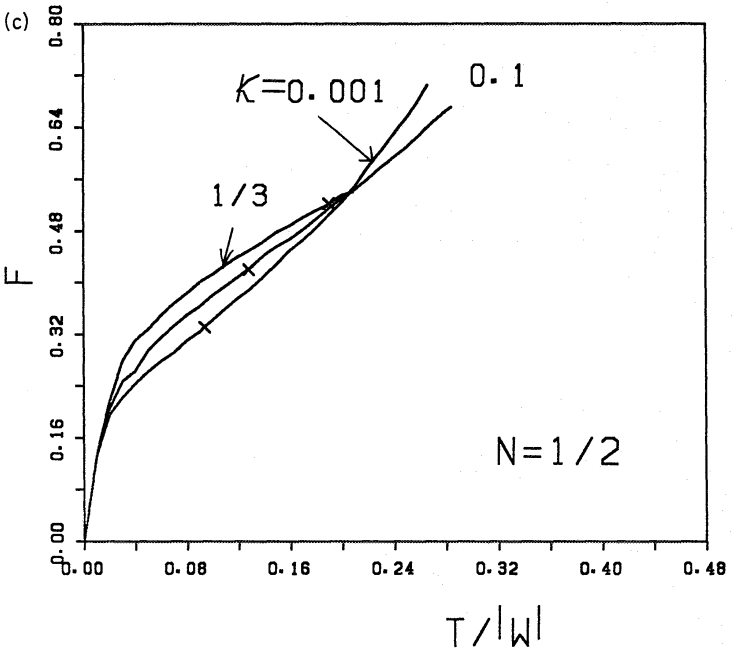

Figure 5 – *continued*

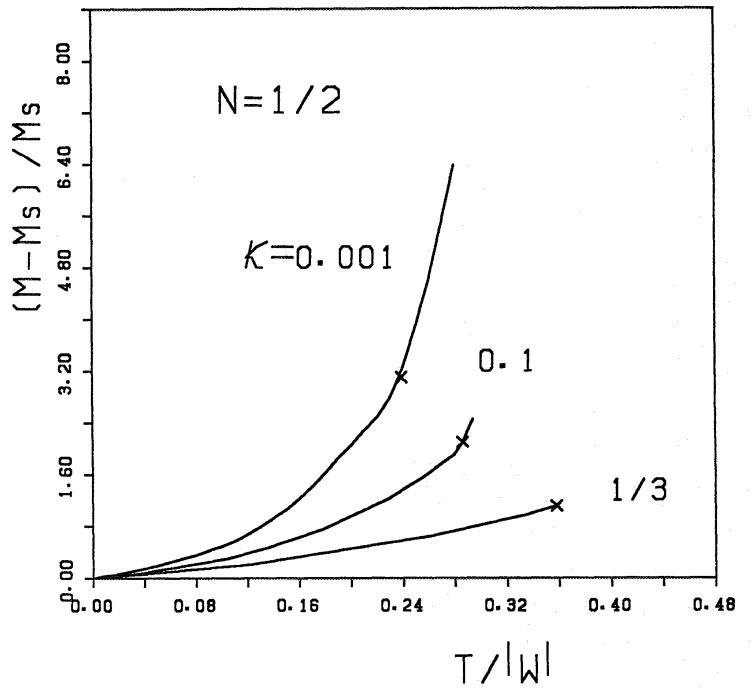

Figure 6. Same as Fig. 3, but for $N=1/2$ sequences. The rotation laws are those for the nearly rigid rotation. The increase in the gravitational mass is affected mainly by the strength of gravity κ and hardly by the rotation parameter A.

case. The qualitative behaviour of the gravitational mass increase is essentially the same as that for the $N=3/2$ case mentioned earlier.

The dragging of the inertial frame ω/Ω is plotted against r/r_e in Fig. 7 for two models on sequence number 13, i.e. for models having $r_p/r_e=0$ and $r_p/r_e=0.9$. The dragging of the rapidly rotating model is larger everywhere than that of the slowly rotating model because the

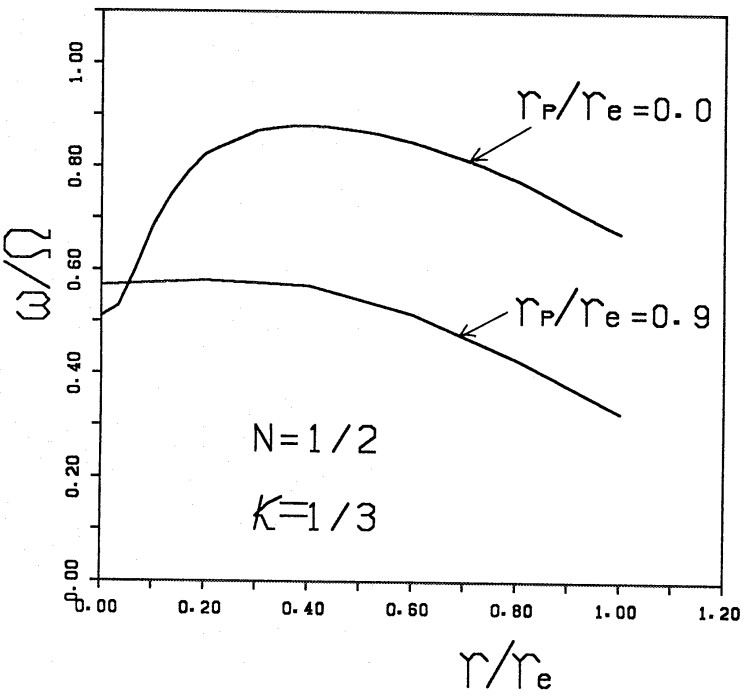

Figure 7. The dragging of the inertial frame ω/Ω in the equatorial plane is plotted against the radius r/r_c for two models having $N=1/2$, i.e. models at $r_p/r_c=0$ and at $r_p/r_c=0.9$. Their rotation is nearly uniform.

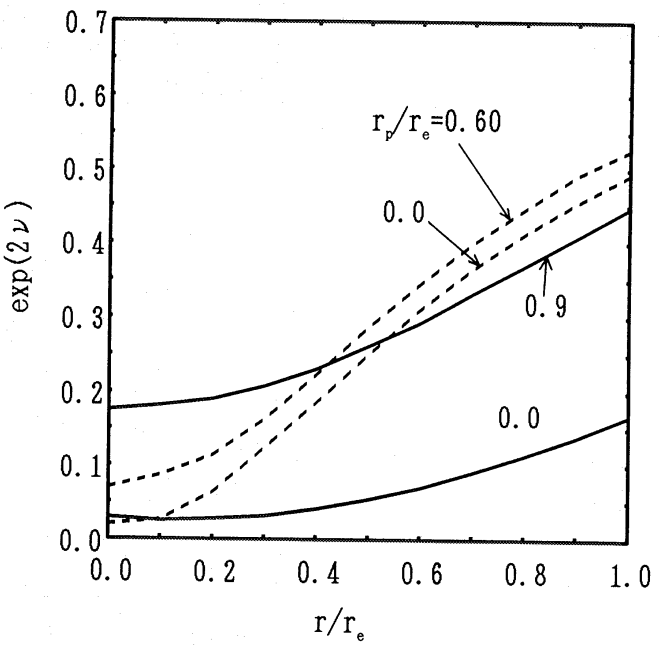

Figure 8. The metric coefficient $e^{2\nu}$ in the equatorial plane is plotted against the radial coordinate in units of the equatorial radius r_c. The solid curves represent the models with $N=1/2$ and $\kappa=1/3$ (on sequence number 13) and the dashed curves the models with $N=3/2$ and $\kappa=0.4$ (on sequence number 10). The values of the axis ratio r_p/r_c are attached to each curve.

strength of gravity M/r_e increases: the gravitational mass M increases but the equatorial radius r_e remains nearly constant.

The metric potentials $e^{2\nu}$ and $e^{2\beta}$ in the equatorial plane are drawn against r/r_e in Figs 8 and 9 for the nearly rigid rotation case. For comparison, the same quantities for the $N=3/2$

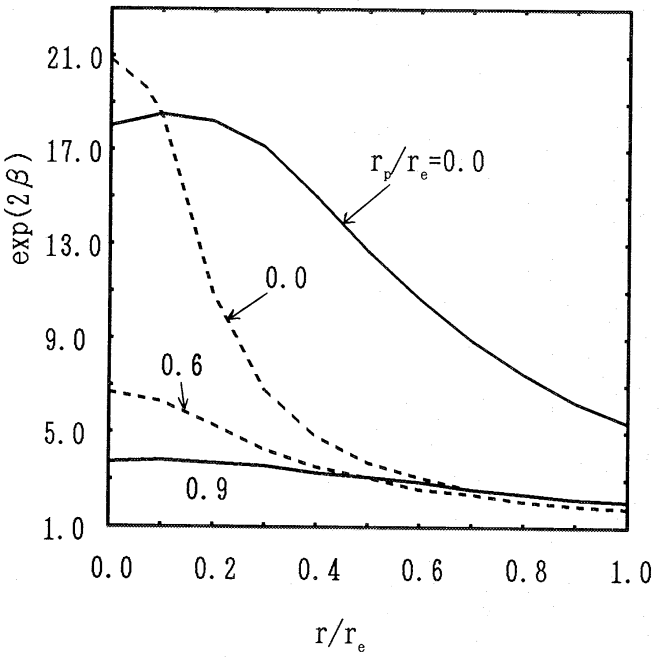

Figure 9. Same as Fig. 8, but for $e^{2\beta}$.

polytrope with strongly differential rotation are also plotted. Larger difference of the values of potentials appears for the $N=3/2$ models than for the $N=1/2$ models between the surface and the coordinate centre, which reflects the difference of the density distribution.

Finally, we tabulate various physical quantities in Table 2 for some selected sequences.

Table 2(a). $N=3/2$ $\kappa=0.001$ $A=0.065$ (sequence number 1).

r_p/r_e	ℓ^2	$\lvert W\rvert\varepsilon_{max}^{1/2}$	F	$M\varepsilon_{max}^{1/2}$	$r_e\varepsilon_{max}^{1/2}$	$T/\lvert W\rvert$	$\frac{\Omega^*_{c(i)}}{\varepsilon_{max}^{1/2}}$
1.0	0.0	1.50E-7	0.0	9.50E-5	5.13E-2	0.0	0.0
0.9	1.09E-2	1.69E-7	0.247	1.02E-4	5.51E-2	2.62E-2	0.461
0.8	2.00E-2	1.86E-7	0.314	1.09E-4	5.83E-2	4.56E-2	0.600
0.7	3.74E-2	2.22E-7	0.409	1.22E-4	6.42E-2	7.87E-2	0.774
0.6	5.27E-2	2.59E-7	0.476	1.34E-4	6.92E-2	0.104	0.881
0.5	7.80E-2	3.36E-7	0.576	1.58E-4	7.70E-2	0.142	1.02
0.4	0.122	6.13E-7	0.746	2.28E-4	8.70E-2	0.204	1.27
0.3	0.152	1.32E-6	0.904	3.53E-4	8.91E-2	0.251	1.54
0.2	0.184	1.71E-6	1.02	4.30E-4	9.22E-2	0.265	1.51
0.1	0.193	1.80E-6	1.05	4.49E-4	9.39E-2	0.266	1.49
0.0	0.197	1.83E-6	1.06	4.57E-4	9.48E-2	0.267	1.49
-0.1	0.202	1.88E-6	1.08	4.67E-4	9.59E-2	0.267	1.45
-0.2	0.215	2.00E-6	1.12	4.91E-4	9.86E-2	0.270	1.38
-0.3	0.252	2.37E-6	1.23	5.64E-4	1.07E-1	0.277	1.22
-0.4	0.294	2.81E-6	1.35	6.45E-4	1.17E-1	0.285	1.08
-0.5	0.395	3.96E-6	1.61	8.45E-4	1.41E-1	0.301	0.834

*For toroidal models, the angular velocity at the inner edge is tabulated.
Negative values of r_p/r_e represent the ratio of the inner radius to the equatorial radius of toroidal models.
l^2 is the squared non-dimensional angular momentum (see Paper I for an exact definition).

Table 2(b). $N=3/2$ $\kappa=0.1$ $A=0.6$ (sequence number 3).

r_p/r_e	ℓ^2	$r_e\varepsilon_{max}^{1/2}$	F	$M\varepsilon_{max}^{1/2}$	$M_p\varepsilon_{max}^{1/2}$	$T/\|W\|$	$\frac{\Omega_{c(i)}}{\varepsilon_{max}^{1/2}}$
1.0	0.0	0.375	0.0	5.23E-2	5.91E-2	0.0	0.0
0.9	1.37E-2	0.397	0.244	5.51E-2	6.23E-2	2.58E-2	0.463
0.8	2.47E-2	0.415	0.308	5.74E-2	6.50E-2	4.47E-2	0.604
0.7	4.46E-2	0.449	0.393	6.18E-2	7.00E-2	7.60E-2	0.779
0.6	6.07E-2	0.479	0.448	6.56E-2	7.44E-2	9.91E-2	0.883
0.5	8.49E-2	0.527	0.522	7.17E-2	8.15E-2	0.131	1.01
0.4	0.122	0.610	0.622	8.26E-2	9.42E-2	0.175	1.17
0.3	0.153	0.683	0.705	9.42E-2	0.108	0.210	1.30
0.25	0.180	0.738	0.780	0.108	0.124	0.242	1.45
0.2	0.199	0.821	0.844	0.123	0.143	0.270	1.64
0.15	0.222	0.421	0.976	0.169	0.205	0.315	2.05
0.1	0.226	0.413	0.992	0.175	0.212	0.316	2.06
0.0	0.229	0.407	1.01	0.180	0.218	0.317	2.07
-0.1	0.236	0.403	1.03	0.189	0.230	0.319	1.95
-0.2	0.250	0.398	1.09	0.209	0.256	0.324	1.73

Table 2(c). $N=3/2$ $\kappa=0.001$ $A=0.0125$ (sequence number 7).

r_p/r_e	ℓ^2	$\|W\|\varepsilon_{max}^{1/2}$	F	$M\varepsilon_{max}^{1/2}$	$r_e\varepsilon_{max}^{1/2}$	$T/\|W\|$	$\frac{\Omega_{c(i)}}{\varepsilon_{max}^{1/2}}$
0.9	6.28E-3	1.81E-7	0.202	1.05E-4	5.22E-2	2.18E-2	1.68
0.8	1.10E-2	2.12E-7	0.254	1.14E-4	5.27E-2	3.76E-2	2.30
0.7	1.90E-2	2.63E-7	0.322	1.29E-4	5.41E-2	6.27E-2	3.17
0.6	2.49E-2	3.02E-7	0.363	1.40E-4	5.52E-2	7.97E-2	3.72
0.5	3.26E-2	3.54E-7	0.412	1.54E-4	5.69E-2	9.98E-2	4.39
0.4	4.16E-2	4.19E-7	0.464	1.72E-4	5.90E-2	0.120	5.13
0.3	4.70E-2	4.60E-7	0.493	1.83E-4	6.04E-2	0.131	5.56
0.2	5.33E-2	5.08E-7	0.526	1.95E-4	6.20E-2	0.141	6.04
0.1	5.58E-2	5.29E-7	0.539	2.00E-4	6.26E-2	0.145	6.24
0.0	5.70E-2	5.39E-7	0.544	2.03E-4	6.29E-2	0.147	6.33
-0.1	6.70E-2	6.17E-7	0.592	2.23E-4	6.55E-2	0.160	5.55
-0.2	9.06E-2	8.09E-7	0.695	2.68E-4	7.12E-2	0.185	4.31
-0.3	0.155	1.36E-6	0.931	3.87E-4	8.65E-2	0.230	2.62
-0.4	0.218	1.98E-6	1.13	5.06E-4	0.101	0.257	1.84
-0.5	0.351	3.44E-6	1.50	7.64E-4	0.132	0.291	1.09

Table 2(d). $N=3/2$ $\kappa=0.4$ $A=0.4$ (sequence number 10).

r_p/r_e	ℓ^2	$r_e\varepsilon_{max}^{1/2}$	F	$M\varepsilon_{max}^{1/2}$	$M_p\varepsilon_{max}^{1/2}$	$T/\|W\|$	$\frac{\Omega_{c(i)}}{\varepsilon_{max}^{1/2}}$
1.0	0.0	0.508	0.0	0.149	0.199	0.0	0.0
0.9	2.03E-2	0.512	0.213	0.152	0.203	2.33E-2	0.778
0.8	3.62E-2	0.514	0.265	0.155	0.206	4.08E-2	1.05
0.7	6.47E-2	0.516	0.330	0.160	0.212	7.07E-2	1.42
0.6	8.73E-2	0.517	0.369	0.163	0.217	9.33E-2	1.68
0.5	0.120	0.518	0.415	0.169	0.224	0.125	2.03
0.4	0.168	0.520	0.470	0.178	0.234	0.168	2.51
0.3	0.204	0.523	0.506	0.185	0.243	0.199	2.89
*0.2	0.265	0.535	0.560	0.199	0.260	0.249	3.60
*0.1	0.307	0.560	0.595	0.210	0.273	0.280	4.19
*0.0	0.343	0.631	0.626	0.221	0.287	0.305	4.82

*Models which have ergo region.

Table 2(e). $N=1/2$ $\kappa=0.001$ $A=0.036$ (sequence number 11).

r_p/r_e	ℓ^2	$\lvert W\rvert\varepsilon_{max}^{1/2}$	F	$M\varepsilon_{max}^{1/2}$	$r_e\varepsilon_{max}^{1/2}$	$T/\lvert W\rvert$	$\frac{\Omega_{c(i)}}{\varepsilon_{max}^{1/2}}$
1.0	0.0	8.41E-8	0.0	6.17E-5	2.99E-2	0.0	0.0
0.9	1.12E-2	1.01E-7	0.254	6.87E-5	3.21E-2	3.22E-2	0.716
0.8	2.04E-2	1.17E-7	0.308	7.52E-5	3.39E-2	5.56E-2	0.941
0.7	3.72E-2	1.55E-7	0.374	8.93E-5	3.72E-2	9.36E-2	1.23
0.6	5.06E-2	1.99E-7	0.414	1.04E-4	4.00E-2	0.121	1.42
0.5	6.91E-2	3.03E-7	0.462	1.34E-4	4.43E-2	0.156	1.68
0.4	9.29E-2	4.97E-7	0.513	1.82E-4	5.01E-2	0.195	1.99
0.3	0.109	6.20E-7	0.542	2.11E-4	5.35E-2	0.216	2.14
0.2	0.127	7.46E-7	0.572	2.40E-4	5.74E-2	0.235	2.24
0.1	0.133	7.85E-7	0.582	2.50E-4	5.88E-2	0.238	2.26
0.0	0.135	7.97E-7	0.585	2.53E-4	5.92E-2	0.239	2.26
-0.1	0.137	8.07E-7	0.588	2.56E-4	5.98E-2	0.239	2.19
-0.2	0.144	8.45E-7	0.598	2.66E-4	6.14E-2	0.241	2.07
-0.3	0.167	9.92E-7	0.630	3.02E-4	6.68E-2	0.250	1.80
-0.4	0.195	1.18E-6	0.665	3.45E-4	7.31E-2	0.259	1.57
-0.5	0.267	1.69E-6	0.741	4.55E-4	8.90E-2	0.279	1.20

Table 2(f). $N=1/2$ $\kappa=1/3$ $A=0.55$ (sequence number 13).

r_p/r_e	ℓ^2	$r_e\varepsilon_{max}^{1/2}$	F	$M\varepsilon_{max}^{1/2}$	$M_p\varepsilon_{max}^{1/2}$	$T/\lvert W\rvert$	$\frac{\Omega_{c(i)}}{\varepsilon_{max}^{1/2}}$
1.0	0.0	0.246	0.0	9.40E-2	0.120	0.0	0.0
0.9	1.69E-2	0.253	0.326	0.101	0.127	4.15E-2	0.820
0.8	3.03E-2	0.256	0.392	0.105	0.134	7.19E-2	1.09
0.7	5.37E-2	0.260	0.470	0.115	0.146	0.122	1.45
0.6	7.14E-2	0.260	0.515	0.124	0.157	0.158	1.69
0.5	9.52E-2	0.254	0.566	0.137	0.175	0.206	2.02
*0.4	0.123	0.241	0.615	0.156	0.199	0.262	2.47
*0.3	0.140	0.231	0.640	0.169	0.215	0.296	2.77
*0.25	0.150	0.223	0.653	0.178	0.226	0.318	2.99
*0.20	0.158	0.216	0.663	0.186	0.236	0.335	3.18
*0.15	0.162	0.213	0.668	0.191	0.241	0.344	3.28
*0.10	0.165	0.210	0.671	0.194	0.246	0.351	3.37
*0.00	0.168	0.207	0.674	0.198	0.250	0.358	3.46

*Models which have ergo region.

Table 2(g). $N=1/2$ $\kappa=0.001$ $A=0.0064$ (sequence number 17).

r_p/r_e	ℓ^2	$\lvert W\rvert\varepsilon_{max}^{1/2}$	F	$M\varepsilon_{max}^{1/2}$	$r_e\varepsilon_{max}^{1/2}$	$T/\lvert W\rvert$	$\frac{\Omega_{c(i)}}{\varepsilon_{max}^{1/2}}$
0.9	3.70E-3	1.08E-7	0.180	7.13E-5	3.14E-2	1.68E-2	3.18
0.8	6.25E-3	1.22E-7	0.213	7.63E-5	3.22E-2	2.78E-2	4.26
0.7	1.02E-2	1.40E-7	0.249	8.30E-5	3.34E-2	4.39E-2	5.65
0.6	1.28E-2	1.52E-7	0.268	8.71E-5	3.41E-2	5.40E-2	6.49
0.5	1.60E-2	1.66E-7	0.288	9.20E-5	3.50E-2	6.55E-2	7.42
0.4	1.96E-2	1.81E-7	0.307	9.72E-5	3.60E-2	7.71E-2	8.39
0.3	2.15E-2	1.90E-7	0.317	1.00E-4	3.65E-2	8.33E-2	8.92
0.2	2.38E-2	2.00E-7	0.327	1.04E-4	3.72E-2	8.97E-2	9.51
0.1	2.47E-2	2.05E-7	0.331	1.05E-4	3.74E-2	9.23E-2	9.75
0.0	2.51E-2	2.07E-7	0.333	1.06E-4	3.75E-2	9.34E-2	9.86
-0.1	3.16E-2	2.39E-7	0.359	1.17E-4	3.94E-2	0.109	8.34
-0.2	4.77E-2	3.19E-7	0.412	1.41E-4	4.35E-2	0.139	6.18
-0.3	9.29E-2	5.51E-7	0.516	2.05E-4	5.37E-2	0.193	3.61
-0.4	0.138	8.15E-7	0.591	2.70E-4	6.34E-2	0.225	2.51
-0.5	0.234	1.46E-6	0.709	4.12E-4	8.38E-2	0.266	1.48

Table 2(h). $N=1/2$ $\kappa=1/3$ $A=0.16$ (sequence number 19).

r_p/r_e	ℓ^2	$r_e\varepsilon_{max}^{1/2}$	F	$M\varepsilon_{max}^{1/2}$	$M_p\varepsilon_{max}^{1/2}$	$T/\|W\|$	$\frac{\Omega_{c(i)}}{\varepsilon_{max}^{1/2}}$
0.9	8.75E-3	0.246	0.266	9.96E-2	0.127	2.61E-2	1.97
0.8	1.52E-2	0.245	0.316	0.103	0.131	4.44E-2	2.66
0.7	2.57E-2	0.244	0.373	0.107	0.137	7.28E-2	3.60
0.6	3.32E-2	0.244	0.404	0.110	0.141	9.22E-2	4.20
0.5	4.29E-2	0.243	0.437	0.114	0.146	0.116	4.94
0.4	5.45E-2	0.242	0.471	0.119	0.152	0.143	5.82
0.3	6.17E-2	0.241	0.489	0.123	0.156	0.160	6.38
0.2	7.06E-2	0.239	0.510	0.127	0.162	0.179	7.10
0.1	7.45E-2	0.239	0.519	0.129	0.164	0.187	7.43
0.0	7.63E-2	0.238	0.522	0.130	0.165	0.190	7.58
-0.05	8.58E-2	0.236	0.542	0.135	0.172	0.209	6.73

3 Discussion

3.1 ROTATION LAWS

In the present paper, we have assumed the rotation law defined by equation (17) of Paper I. However, the specific angular momentum $\tilde{j}$ defined by

$$\tilde{j}=u_\phi(\varepsilon+p)/\rho_0 \tag{2}$$

is much more important because $\tilde{j}$ is a locally conserved quantity, but j defined by equation (16) of Paper I is not, during axisymmetric collapses of perfect fluids. Here, u_ϕ and ρ_0 are the ϕ-component of the four-velocity and the rest mass density, respectively. This conserved specific angular momentum is related to the specific angular momentum measured by the proper time, j, as follows, if we assume the isentropy throughout the star (Bardeen 1970):

$$\tilde{j}(\Omega)=-e^C\frac{\partial}{\partial\Omega}\exp\left[-\int^{\Omega}j(\Omega)\,d\Omega\right], \tag{3}$$

where C is an integration constant. Taking the functional form of $j(\Omega)$ defined by equation (17) of Paper I, we obtain

$$\tilde{j}(\Omega)=e^C A^2(\Omega_c-\Omega)\exp[A^2(\Omega-\Omega_c)^2/2], \tag{4}$$

and

$$d\tilde{j}/d\Omega=-A^2[1+A^2(\Omega-\Omega_c)^2]\exp[A^2(\Omega-\Omega_c)^2/2+C]. \tag{5}$$

Thus, $d\tilde{j}/d\Omega$ is always negative. Therefore, rotation law (4) or (17) of Paper I satisfies the generalized Rayleigh's criterion against axisymmetric disturbances, although this criterion cannot exclude the possibility of non-axisymmetric instabilities demonstrated first by Papaloizou & Pringle (1984) in the Newtonian limit.

3.2 ERGO REGION

We can observe the appearance of ergo regions, in which any observer must rotate relative to infinity, for the case of rapid rotation and strong gravity ($\kappa\geq 0.2$). Fig. 10 shows such examples. Appearance and growing of the ergo region are qualitatively the same as in the results computed by Wilson (1972) and Butterworth & Ipser (1975). When an ergo region appears, relativistic instabilities against non-axisymmetric modes of $e^{im\phi}$ are induced for sufficiently

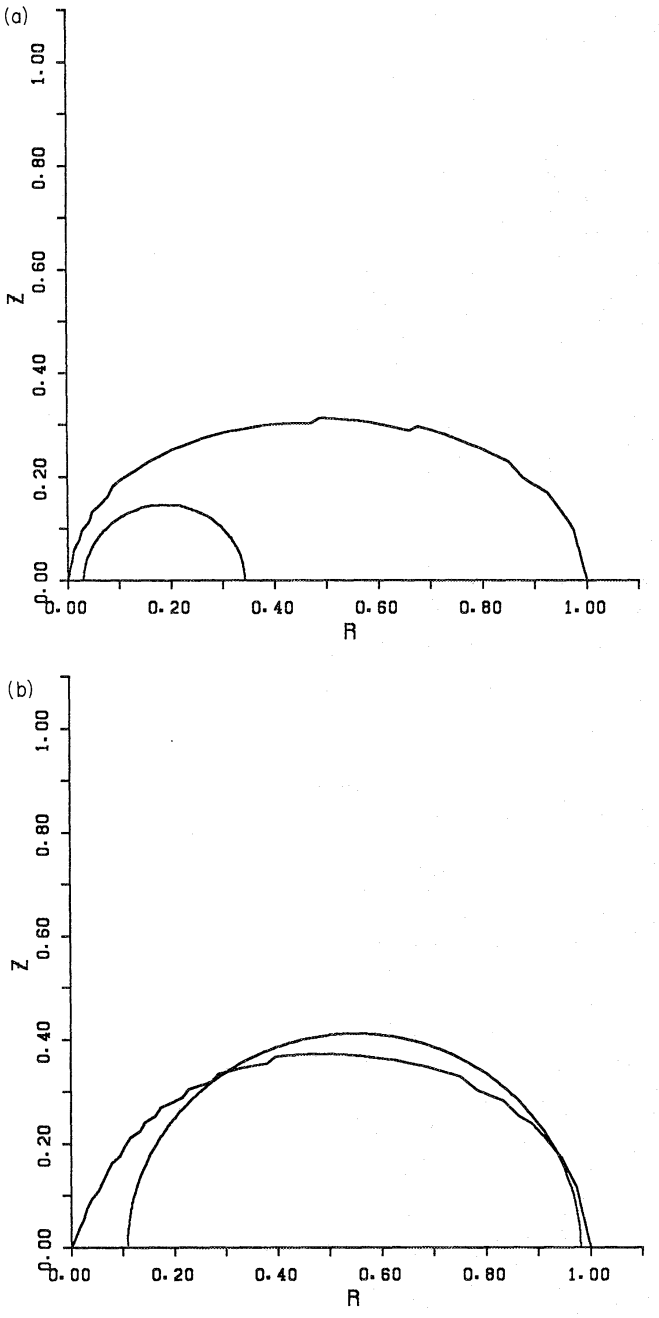

Figure 10. The boundary of the ergo region is shown for two cases corresponding to the models shown in (a) Fig. 1(c), and (b) Fig. 4(a). Matter surfaces are also plotted.

large m because, observed from infinity, negative energy states appear into which matter can fall, emitting a gravitational wave (Butterworth & Ipser 1976; Friedman 1978). This instability has been studied by Comins & Schutz (1978). They have proved that the e-folding time for the growing mode is huge for high mode number m and for slow rotation. Thus we need not care about this instability but should consider the secular instability due to the gravitational wave radiation (Chandrasekhar 1970; Friedman & Schutz 1978). However, we will not discuss stability of the observed models in this paper. The models having an ergo region are denoted by asterisks in Table 2.

3.3 NUMERICAL ACCURACY CHECK

We have checked the numerical accuracy by doubling the number of mesh points in the angular direction and the cut-off number of Legendre and triangular functions in the expansion series of Green's functions (33), (34) and (35) of Paper I. The number of mesh points and the number of Legendre functions have a direct influence on the potentials such as ν, α, β and ω. However, the potentials and other physical quantities of the two results for ring-like structures are in agreement with each other to within 1 per cent. Considering other accuracy checks mentioned in Paper I, we may conclude that our results are correct to within a few per cent.

Acknowledgments

One of us, HK, would like to thank Professor Yoji Osaki for his encouragements. We would like to thank the referee who pointed out the paper by Comins & Schutz. Numerical computations were carried out on a Fujitsu M-380R at the Tokyo Astronomical Observatory. This research was supported in part by the Grant-in-Aid for Scientific Research (62540183, 63540190) of the Ministry of Education, Science and Culture in Japan.

References

Bardeen, J. M., 1970. *Astrophys. J.*, **162,** 71.
Butterworth, E. M. & Ipser, J. R., 1975. *Astrophys. J.*, **200,** L103.
Butterworth, E. M. & Ipser, J. R., 1976. *Astrophys. J.*, **204,** 200.
Chandrasekhar, S., 1970. *Phys. Rev. Lett.*, **24,** 611.
Comins, N. & Schutz, B. F., 1978. *Proc. Roy. Soc. London A*, **364,** 211.
Eriguchi, Y. & Hachisu, I., 1985. *Astr. Astrophys.*, **148,** 289.
Eriguchi, Y. & Müller, E., 1985. *Astr. Astrophys.*, **147,** 161.
Eriguchi, Y. & Sugimoto, D., 1981. *Prog. theor. Phys.*, **65,** 1870.
Friedman, J. L., 1978. *Comms. Math. Phys.*, **63,** 243.
Friedman, J. L. & Schutz, B. F., 1978. *Astrophys. J.*, **222,** 281.
Friedman, J. L., Ipser, J. R. & Parker, L., 1986. *Astrophys. J.*, **304,** 115.
Hachisu, I., 1986. *Astrophys. J. Suppl.*, **61,** 479.
Hachisu, I., Tohline, J. E. & Eriguchi, Y., 1987. *Astrophys. J.*, **323,** 592.
Hachisu, I., Tohline, J. E. & Eriguchi, Y., 1988. *Astrophys. J. Suppl.*, **66,** 315.
Hirata, K. *et al.*, 1987. *Phys. Rev. Lett.*, **58,** 1490.
Komatsu, H., Eriguchi, Y. & Hachisu, I., 1989. *Mon. Not. R. astr. Soc.*, **237,** 355 (Paper I).
Nakamura, T., 1981. *Prog. theor. Phys.*, **65,** 1876.
Nakamura, T. & Fukugita, M., 1987. Preprint.
Papaloizou, J. C. B. & Pringle, J. E., 1984. *Mon. Not. R. astr. Soc.*, **208,** 721.
Stark, R. F. & Piran, T., 1985. *Phys. Rev. Lett.*, **55,** 891.
Symbalisty, E. D., 1984. *Astrophys. J.*, **285,** 729.
Tohline, J. E., 1984. *Astrophys. J.*, **285,** 721.
Wilson, J. R., 1972. *Astrophys. J.*, **176,** 195.
Wilson, J. R., 1973. *Phys. Rev. Lett.*, **30,** 1082.